Journal of Alloys and Compounds 501 (2010) 269–274

Contents lists available at ScienceDirect

Journal of Alloys and Compounds

journal homepage: www.elsevier.com/locate/jallcom

Thermodynamic and transport properties of the $PrBr_3$–RbBr binary system

Leszek Rycerz [a], Ewa Ingier-Stocka [a], Madjid Berkani [b], Marcelle Gaune-Escard [c,*]

[a] Chemical Metallurgy Group, Faculty of Chemistry, Wroclaw University of Technology, Wybrzeze Wyspianskiego 27, 50-370 Wroclaw, Poland
[b] Laboratoire de Génie de l'Environnement, Département de Chimie, Faculté des Sciences Exactes, Université A. Mira, Béjaïa 06000, Algeria
[c] Ecole Polytechnique, IUSTI CNRS UMR 6595, Technopole de Chateau-Gombert, 5 rue Enrico Fermi, 13453 Marseille Cedex 13, France

ARTICLE INFO

Article history:
Received 27 October 2009
Received in revised form 8 April 2010
Accepted 14 April 2010
Available online 24 April 2010

Keywords:
Inorganic materials
Electrical transport
Phase diagrams
Thermodynamic properties
Calorimetry
Thermal analysis

ABSTRACT

Phase equilibrium in the $PrBr_3$–RbBr binary system was established by differential scanning calorimetry (DSC). This system, investigated for the first time, includes Rb_3PrBr_6, Rb_2PrBr_5 and $RbPr_2Br_7$ compounds, and three eutectics located at molar fraction of $PrBr_3$ ($x = 0.136$; 865 K), ($x = 0.488$; 765 K) and ($x = 0.679$; 834 K), respectively. Rb_3PrBr_6 undergoes a solid–solid phase transition at 704 K and melts congruently at 995 K. Rb_2PrBr_5 melts incongruently at 803 K and finally $RbPr_2Br_7$ melts congruently at 852 K. The electrical conductivity of $PrBr_3$–RbBr liquid mixtures was measured over an extended temperature range down to temperatures below solidification and over the whole composition range. Results obtained are discussed in terms of possible complex formation.

1. Introduction

Lanthanide halides play a very important role in many technological applications. They are extensively used in optical and scintillation [1–5] devices and are attractive components for doses in high-intensity discharge lamps and new highly efficient light sources with energy saving features [6]. The wide band gap materials like fluorides and other halides co-doped by lanthanide ions provide valuable insight into many aspects of luminescence centers and have wide applications [7]. The development of new phosphors for vacuum ultraviolet (VUV) excitation is an important new challenge in the field of luminescence materials research. The phosphors excited in the VUV can be used in a new generation of lamps or in gas plasma discharge devices for flat color display panels. Praseodymium and cerium compounds seem to be promising for these purposes [7]. In spite of the technological importance, the properties of many lanthanide halides, however, are poorly characterised. Bromides have received even less attention in scientific literature than chlorides and iodides. Comprehensive thermochemical parameters for the lanthanide tribromides are not available in any of the standard compilations of thermodynamic properties. These properties are required for the calculation of the chemical composition in the lamp to assist in the understanding and hence prediction of tungsten corrosion, silica corrosion and spectral output. The data are also needed for predicting the behaviour of doses by modelling multicomponent metal halide systems [8].

In connection with our research program on lanthanide halides and their systems with alkali metal halides, aiming to determine the physicochemical properties of these poorly characterised LnX_3–MX systems, we have investigated the binary system of praseodymium(III) bromide with rubidium bromide.

In addition to investigating one more system in this systematic research program, our goal was also to further test systematic rules evidenced recently [9] from our own investigations and literature data regarding the topology of related phase diagrams. As reported previously [9] a relation between the phase diagram topology and the physicochemical properties of components was established in the LnX_3–MX systems. The so-called "ionic potential", $IP = e_i/r_i$, where r_i = ionic radius, $e_i = Z_i\varepsilon$ (Z_i = valency and ε = elementary charge), was found to be an important parameter in this respect. The "ionic potential" is a measure of the electric field intensity at the cation surface, therefore accounting for interaction forces between cations with anions. The ratio of ionic potential of the alkali metal cation and the lanthanide cation, IP_{M+}/IP_{Ln3+}, expresses a comparison of the interaction energies and influences the phase diagram topology of LnX_3–MX binary systems. When $IP_{M+}/IP_{Ln3+} \leq 0.256$, both incongruently and congruently melting compounds are present in the systems.

This had been previously tested on the $CeBr_3$–MBr binary systems (M = Li, Na, K, Rb), still unknown at that time. Indeed it was found that $CeBr_3$–LiBr and $CeBr_3$–NaBr are simple eutec-

* Corresponding author. Tel.: +33 4 91 10 68 87; fax: +33 4 91 11 74 39.
E-mail addresses: leszek.rycerz@pwr.wroc.pl (L. Rycerz), berkanima@yahoo.fr (M. Berkani), marcelle.gaune-escard@polytech.univ-mrs.fr, molten.salts@polytech.univ-mrs.fr (M. Gaune-Escard).

0925-8388/$ – see front matter © 2010 Elsevier B.V. All rights reserved.
doi:10.1016/j.jallcom.2010.04.087

tic systems [10] (IP_{M+}/IP_{Ce3+} = 0.465 and 0.366, respectively), whereas in the system $CeBr_3$–KBr [11] two congruently melting compounds, namely K_3CeBr_6 and K_2CeBr_5 exist in agreement with the above observation (IP_{K+}/IP_{Ce3+} = 0.249). Therefore the $CeBr_3$–RbBr binary system followed the expected behaviour and since IP_{Rb+}/IP_{Ce3+} = 0.231, three compounds are formed accordingly in this system [12]. One of them (Rb_2CeBr_5) melts incongruently, whereas the other two (Rb_3CeBr_6 and $RbCe_2Br_7$) melt congruently. $PrBr_3$-based bromide systems follow this trend. The binary systems with LiBr and NaBr are of simple eutectic-type [13] (IP_{M+}/IP_{Pr3+} = 0.456 and 0.330, respectively). In the system with KBr [14], the congruently melting compound, K_3PrBr_6 and two incongruently melting compounds (K_2PrBr_5 and KPr_2Br_7) were found (IP_{K+}/IP_{Pr3+} = 0.244). It can be expected that the system with rubidium bromide (IP_{Rb+}/IP_{Pr3+} = 0.227) would be characterised by analogous compounds.

In addition the electrical conductivity of $PrBr_3$–RbBr liquid binary mixtures was measured over the whole composition range and a wide temperature range.

2. Experimental

2.1. Chemicals

Praseodymium(III) bromide was synthesised from the praseodymium oxide, Pr_6O_{11}. The main steps of this synthesis include: dissolution of oxide in hot concentrated HBr acid, crystallisation of $PrBr_3{\cdot}nH_2O$, its dehydration in the presence of ammonium bromide, sublimation of NH_4Br, melting of crude $PrBr_3$ and its purification by distillation under reduced pressure (~0.1 Pa) in a quartz ampoule at 1150 K. The details of this synthesis were described elsewhere [13]. $PrBr_3$ prepared in this way was of a high purity – minimum 99.9%. Chemical analysis was performed by mercurimetric (bromine) and complexometric (praseodymium) methods. The results were as follows: Pr, 36.96 ± 0.15% (37.02% theoretical); Br, 63.04 ± 0.11% (62.98% theoretical).

Rubidium bromide was a Merck Suprapur reagent (minimum 99.9%). Before use, it was progressively heated up to fusion under gaseous HBr atmosphere. Excess of HBr was then removed from the melt by argon bubbling.

Table 1
Compositions of $PrBr_3$–RbBr mixtures used in DSC measurements.

Sample no.	$m(PrBr_3)$ (g)	m(RbBr) (g)	$x(PrBr_3)$
1	0.0971	1.6340	0.025
2	0.2233	1.8463	0.050
3	0.1937	1.0206	0.076
4	0.4109	1.600	0.100
5	0.2567	0.7694	0.127
6	0.5325	1.3254	0.149
7	0.4777	0.9614	0.177
8	0.7647	1.3311	0.200
9	0.5973	0.8330	0.237
10	0.2010	0.2620	0.250
11	0.4832	0.5654	0.271
12	0.5073	0.5210	0.297
13	0.7381	0.7026	0.313
14	0.6959	0.5623	0.350
15	0.6812	0.4972	0.373
16	0.6073	0.4044	0.395
17	0.7493	0.4380	0.426
18	0.6789	0.3429	0.462
19	0.7044	0.3052	0.501
20	0.7707	0.3059	0.523
21	0.7428	0.2707	0.544
22	0.8535	0.2717	0.577
23	0.7804	0.2264	0.600
24	0.7430	0.1940	0.625
25	1.0058	0.2337	0.652
26	0.7741	0.1693	0.665
27	0.8021	0.1743	0.666
28	0.7694	0.1592	0.677
29	0.8798	0.1335	0.741
30	1.3528	0.1505	0.796
31	1.4042	0.1076	0.850
32	1.9080	0.0934	0.899
33	2.4464	0.0570	0.949

All chemicals were handled inside a high purity argon atmosphere in a glove box (water content < 2 ppm).

2.2. Measurements

Experimental mixture samples, made from the appropriate amounts of $PrBr_3$ and RbBr (Table 1) were melted in vacuum-sealed quartz ampoules. The melts were homogenised and solidified. These samples were ground in an agate mortar in a glove box. Homogenous mixtures of different compositions were prepared in this way and used in phase diagram measurements.

Phase equilibria in the $PrBr_3$–RbBr system were investigated with a Setaram DSC 121 differential scanning calorimeter. Experimental samples (300–500 mg) were contained in vacuum-sealed quartz ampoules. Experiments were conducted at heating and cooling rates ranging 1–5 K min^{-1}. Details of experimental procedures and apparatus calibration were given previously [13]. The maximum relative experimental error on enthalpy of phase transition did not exceed 1%. Temperature was measured with precision ±1 K.

Electrical conductivity measurements were carried out in the capillary quartz cells described in detail elsewhere [15], and calibrated with molten NaCl [16]. Experimental mixture samples, made from the appropriate amounts of $PrBr_3$ and RbBr were placed in capillary cells and melted under argon atmosphere. The melts were homogenised by argon bubbling during 30 min. The cells constants varied between 11 000 and 12 500 m^{-1}. The change of any individual cell constant was less than 1% after several experiments. The conductivity of the melt was measured by platinum electrodes with the conductivity meter Tacussel CD 810 during increasing and decreasing temperature runs. The mean values of these two runs were used in calculations. Experimental runs were performed at heating and cooling rates 1 K min^{-1}. Temperature was measured with a Pt/Pt–Rh(10) thermocouple with 1 K accuracy. Temperature and conductivity data acquisition were made with PC computer, interfaced to the conductivity meter. All measurements were carried out under static argon atmosphere. The accuracy of measurements was estimated at ±2%.

3. Results and discussion

3.1. Phase diagram

DSC investigations, performed on 35 samples with different compositions, yielded both the corresponding temperature and enthalpy. Due to a frequent supercooling effect, all temperature and enthalpy values reported here were determined from heating curves. Solidus and liquidus temperatures were determined as T_{onset} and T_{peak} of appropriate effects, respectively.

Fig. 1 shows the heating thermograms for samples with molar fraction of $PrBr_3$, x = 0.050, 0.250, 0.297, 0.373, 0.665 and 0.796, respectively, obtained with heating rate 5 K min^{-1}.

In all thermograms, the endothermic effect observed at the highest temperature corresponds to liquidus. In the composition range $0 < x \leq 0.250$, where x is the $PrBr_3$ molar fraction, two additional endothermic peaks were present in all heating thermograms (with the exception of compositions very close to the eutectic). The first one, at 865 K (mean value from measurements), is observable in all thermograms up to $x < 0.250$. Its disappearance at $x = 0.250$ suggests the existence of the Rb_3PrBr_6 compound. It can be undoubtedly ascribed to the RbBr–Rb_3PrBr_6 eutectic. The eutectic composition was determined accurately from the Tamman plot (Fig. 2a). The analysis of this experimental enthalpy *vs.* composition plot evidences that no solid solutions form in the system. Thus the corresponding straight lines intercept the composition axis at $x = 0$ and 0.250. The eutectic composition, $x = 0.136 \pm 0.005$, was determined from the intercept of the two linear parts in Fig. 2a. The eutectic temperature determined from all appropriate DSC curves was found to be 865 ± 1 K, whereas the enthalpy of fusion at the eutectic composition was 15.3 ± 0.3 kJ mol^{-1}.

The second thermal effect at 704 K (mean value for samples of different compositions) in samples with composition range $0 < x \leq 0.250$ was also observed in all samples with $PrBr_3$ molar fraction up to $x < 0.333$, composition at which it disappears. The Tamman construction for this effect (Fig. 2b) evidences that it is related to the Rb_3PrBr_6 compound. The molar enthalpy related to this effect (calculated for the Rb_3PrBr_6 compound), $\Delta H_m = 8.0 \pm 0.4$ kJ mol^{-1}, is in excellent agreement with the

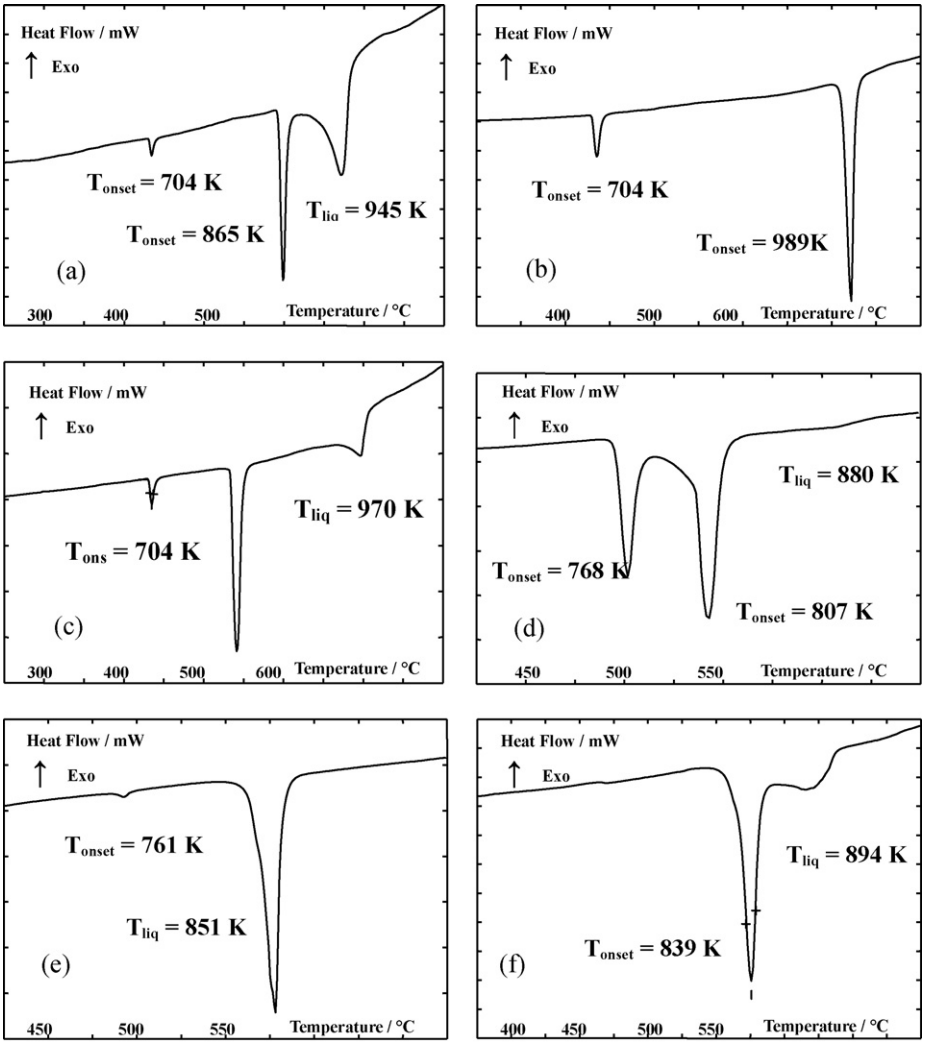

Fig. 1. DSC heating curves for $PrBr_3$–RbBr mixtures of different compositions obtained with heating rate 5 K min^{-1}, $x = 0.050$, 0.250, 0.297, 0.373, 0.665 and 0.796 (x denotes mole fraction of $PrBr_3$).

enthalpy observed previously [9] for many M_3LnX_6 compounds (M = Rb, Cs; Ln = lanthanide) and ascribed to a solid–solid phase transition. Accordingly, this effect at 704 K was attributed to a solid–solid phase transition in Rb_3PrBr_6.

Two thermal events were observed at 704 K and 995 K for the sample of composition $x = 0.250$ and were related to a solid–solid phase transition (from low-temperature (LT) to high-temperature (HT) modification) and the congruent melting of the Rb_3PrBr_6 compound.

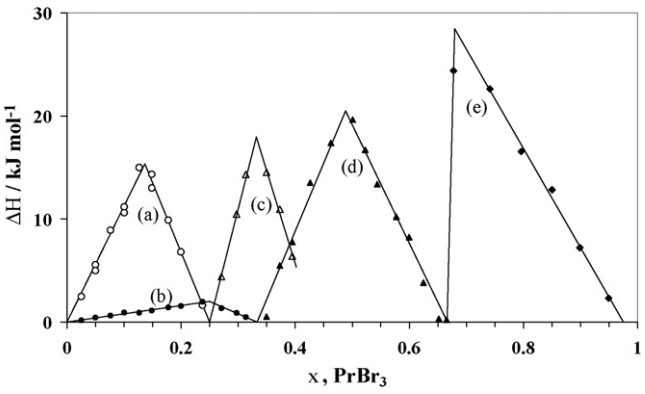

Fig. 2. Tamman constructions for the $PrBr_3$–RbBr system: description in the text.

This thermal event at about 704 K was not detected in samples with $x \geq 0.333$, suggesting the existence of another compound, namely Rb_2PrBr_5. Indeed, an additional thermal effect at 803 K, which appears for samples in the composition range $0.250 < x \approx 0.402$ corresponds to the incongruent melting of Rb_2PrBr_5, which leads to the formation of liquid phase and solid Rb_3PrBr_6. Tamman diagram construction (enthalpy related to the effect at 803 K *vs.* $PrBr_3$ molar fraction) (Fig. 2c) yields the value $x = 0.332 \pm 0.024$, which is in excellent agreement with the theoretical value $x = 0.333$ for Rb_2PrBr_5.

One or two endothermic peaks in addition to liquidus were observed on heating thermograms for the samples in the composition range $0.250 < x < 0.666$. The first one, at 803 K (as mentioned above), corresponds to the incongruent melting of Rb_2PrBr_5. The second one, observable at about 765 K, disappears at compositions $x \geq 0.666$, thus suggesting the existence of another compound, namely $RbPr_2Br_7$. Thus it can be ascribed to the Rb_2PrBr_5–$RbPr_2Br_7$ eutectic. The enthalpy-composition plot in Fig. 2d resulted in the eutectic composition, $x = 0.488 \pm 0.009$. This eutectic mixture melts at 765 K, with the related enthalpy $\Delta_{fus}H_m = 20.5 \pm 0.7$ kJ mol^{-1}.

Only one endothermic effect was observed on heating DSC curves for the mixture of composition $x = 0.666$ at 852 K. It corresponds to the congruent melting of the $RbPr_2Br_7$ compound.

Table 2
DSC results for $PrBr_3$–RbBr binary system.

Sample no.	$x(PrBr_3)$	T/K					
		Rb_3PrBr_6 phase transition	RbBr–Rb_3PrBr_6 eutectic	Rb_2PrBr_5 decomposition	Rb_2PrBr_5–$RbPr_2Br_7$ eutectic	$RbPr_2Br_7$–$PrBr_3$ eutectic	Liquidus
0	0.000	–	–	–	–	–	967
1	0.025	701	864	–	–	–	959
2	0.050	704	865	–	–	–	945
3	0.076	704	866	–	–	–	927
4	0.100	704	866	–	–	–	904
5	0.127	703	864	–	–	–	879
6	0.149	704	865	–	–	–	883
7	0.177	705	866	–	–	–	921
8	0.200	704	865	–	–	–	958
9	0.237	703	863	–	–	–	989
10	0.250	704	–	–	–	–	995
11	0.271	702	–	800	–	–	986
12	0.297	704	–	806	–	–	970
13	0.313	700	–	803	–	–	955
14	0.350	–	–	799	749	–	916
15	0.373	–	–	807	768	–	880
16	0.395	–	–	806	767	–	813
17	0.426	–	–	–	768	–	798
18	0.462	–	–	––	768	–	778
19	0.501	–	–	–	766	–	776
20	0.523	–	–	–	766	–	797
21	0.544	–	–	–	766	–	810
22	0.577	–	–	–	766	–	828
23	0.600	–	–	–	768	–	839
24	0.625	–	–	–	762	–	844
25	0.652	–	–	–	760	–	853
26	0.665	–	–	–	761	–	851
27	0.666	–	–	–	–	–	852
28	0.677	–	–	–	–	838	851
29	0.741	–	–	–	–	838	878
30	0.796	–	–	–	–	839	894
31	0.850	–	–	–	–	837	934
32	0.899	–	–	–	–	833	941
33	0.949	–	–	–	–	817	958
34	1.000	–	–	–	–	–	960

Finally, one effect in addition to the liquidus was observable at about 834 K in mixtures in the range $x > 0.666$. It undoubtedly corresponds to the $RbPr_2Br_7$–$PrBr_3$ eutectic. The enthalpy *vs.* molar fraction $PrBr_3$ (Fig. 2e) gives $x = 0.679 \pm 0.004$ as the eutectic composition. This eutectic mixture melts at 834 K with the related enthalpy 28.5 ± 0.7 kJ mol^{-1}. It should be pointed out that the Tamman diagram for the $RbPr_2Br_7$–$PrBr_3$ eutectic (Fig. 2e) suggests the existence of solid solutions. Accordingly, the straight line on the right hand side does not cross the composition axis at $x = 1$. The $PrBr_3$ molar fractions at which solid solutions may exist at 834 K were found as $x \geq 0.975$.

All the results of DSC investigations are presented in Table 2, and the complete phase diagram is shown in Fig. 3.

3.2. Electrical conductivity

The electrical conductivity of the $PrBr_3$–RbBr liquid mixtures was measured for the first time. Experimental determinations were conducted over the entire composition range in steps of about 10 mol% and on an extended temperature range.

The experimental conductivity, κ, data of the liquid phase were well represented by the equation:

$$\ln(\kappa) = A_0 + A_1\left(\frac{1000}{T}\right) + A_2\left(\frac{1000}{T}\right)^2 \quad (1)$$

where A_0, A_1, and A_2 are coefficients determined by the least-squares method. The activation energy, E_A, evaluated by analogy to the Arrhenius equation as

$$E_A(T) = -R\frac{\mathrm{d}\ \ln(K)}{\mathrm{d}(1000/T)} \quad (2)$$

where R is the gas constant, becomes

$$E_A = -R\left[A_1 + 2A_2\left(\frac{1000}{T}\right)\right] \quad (3)$$

All A_i coefficients are listed in Table 3, together with the E_A values determined at 1050 K for all the $PrBr_3$–RbBr mixtures.

The experimental conductivity isotherm at 1050 K was plotted against the mole fraction of $PrBr_3$ in Fig. 4. Conductivity decreases with the increase of $PrBr_3$ composition, with significantly larger changes in the rubidium bromide-rich region.

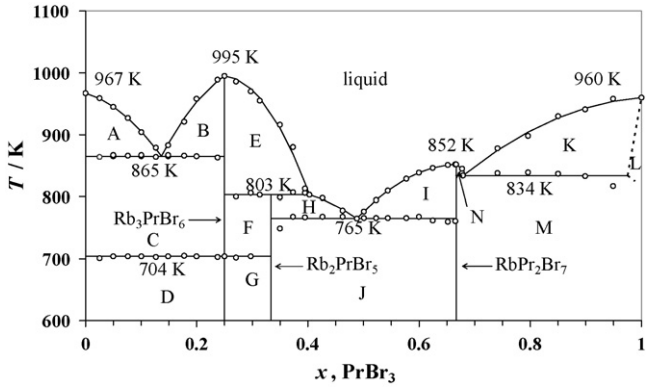

Fig. 3. Phase diagram of the $PrBr_3$–RbBr binary system. Description of phase equilibrium areas: A: $RbBr_{(s)}$ + liquid; B: HT-$Rb_3PrBr_{6(s)}$ + liquid; C: $RbBr_{(s)}$ + HT-$Rb_3PrBr_{6(s)}$; D: $RbBr_{(s)}$ + LT-$Rb_3PrBr_{6(s)}$; E: HT-$Rb_3PrBr_{6(s)}$ + liquid; F: HT-$Rb_3PrBr_{6(s)}$ + $Rb_2PrBr_{5(s)}$; G: LT-$Rb_3PrBr_{6(s)}$ + $Rb_2PrBr_{5(s)}$; H: $Rb_2PrBr_{5(s)}$ + liquid; I: $RbPr_2Br_{7(s)}$ + liquid; J: $Rb_2PrBr_{5(s)}$ + $RbPr_2Br_{7(s)}$; K: solid solution + liquid; L: solid solution; M: $RbPr_2Br_{7(s)}$ + solid solution, and N: $RbPr_2Br_{7(s)}$ + liquid.

Table 3
Coefficients of the electrical conductivity equation: $\ln K = A_0 + A_1(1000/T) + A_2(1000/T)^2$ and the activation energy of the electrical conductivity (E_A) of liquid $PrBr_3$–RbBr binary mixtures at 1050 K: K in S m^{-1}, ln(s) = standard deviation of ln K, and n = number of experimental data points.

$x(PrBr_3)$	Temperature range (K)	A_0 (S m^{-1})	A_1 (S m^{-1} K)	A_2 (S m^{-1} K^2)	ln(s)	n	E_A at 1050 K (kJ/mol)
0.000	993–1124	5.7114	−0.4031	−0.5083	0.0009	386	11.325
0.105	983–1150	4.7608	1.5330	−1.6720	0.0030	361	13.733
0.202	957–1150	4.6902	1.4596	−1.7755	0.0024	397	15.982
0.305	964–1140	5.7835	−1.1299	−0.4408	0.0060	366	16.375
0.431	840–1150	5.0893	0.1843	−1.1487	0.0028	657	16.659
0.537	842–1150	4.4403	1.7218	−2.0230	0.0036	659	17.721
0.636	845–1150	4.1941	2.5414	−2.6468	0.0066	642	20.786
0.718	912–1150	4.0724	2.9421	−2.9510	0.0039	510	22.273
0.847	975–1150	4.7829	1.8151	−2.5374	0.0024	379	25.091
0.945	984–1150	4.7276	2.0123	−2.7467	0.0011	386	26.767
1.000	977–1170	4.9342	1.6942	−2.6688	0.0027	454	28.178

Fig. 5 shows the activation energy at 1050 K as a function of composition. For comparison, the data on activation energy for the analogous system with LiBr [13] are also included in Fig. 5. Whereas in the system with LiBr the activation energy increases smoothly with $PrBr_3$ concentration, in the system with RbBr it increases up to about 15 mol% of $PrBr_3$ and becomes almost stable up to about 55 mol% of $PrBr_3$. This plateau can be explained in terms of coexistence of different forms of complexes as evidenced by Raman spectroscopy [17]. These investigations showed that octahedral $LnBr_6^{3-}$ ions are formed in $LnBr_3$–MBr liquid mixtures. These ions constitute the predominant species in the MBr-rich liquid mixtures. As the $LnBr_3$ concentration increases distorted octahedral species occur, which are bridged by bromide anions. Complex formation in the melt influences the activation energy for electrical conductivity, which should increase with increasing amount of complex formed. The activation energy for electrical conductivity increases with alkali metal cationic radius (from lithium to rubidium). It is likely that this is due to the complex concentration increase in the melt. This observation is in agreement with preliminary mixing enthalpy measurements [18] that also indicate that formation enthalpy, attributed to the $PrBr_6^{3-}$ complex ions formation, increases with ionic radius of alkali metal cation. Thus the presence of RbBr in mixtures with $PrBr_3$ favours complex ion formation more than addition of LiBr and results in a larger enthalpy of formation, larger activation energy for conductivity, etc.

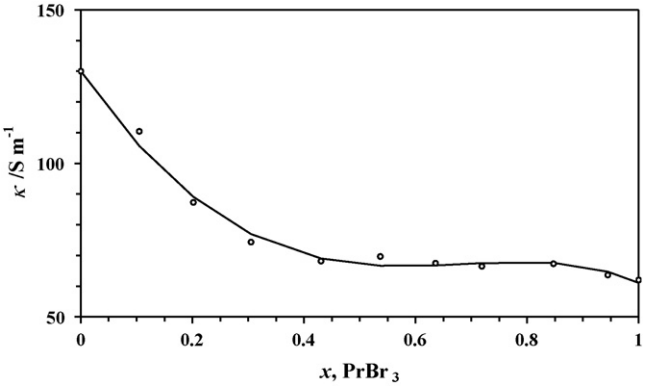

Fig. 4. Electrical conductivity isotherms of $PrBr_3$–RbBr liquid mixtures at 1050 K: (open circles) experimental results; and (solid line) polynomial fitting.

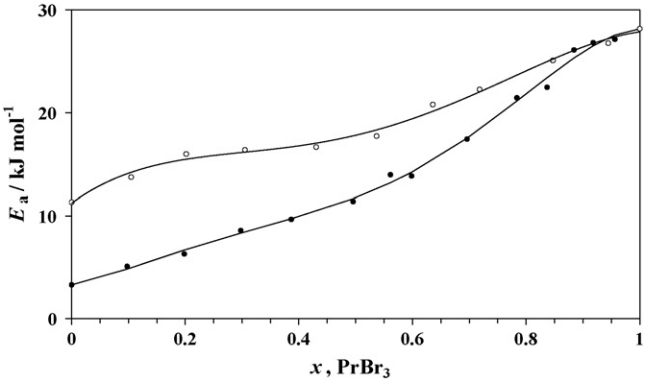

Fig. 5. Activation energy at 1050 K of $PrBr_3$–MBr liquid mixtures: (open circles) M = Rb; (black circles) M = Li; and (solid lines) polynomial fitting.

4. Conclusions

Phase equilibrium in the $PrBr_3$–RbBr binary system was established for the first time by differential scanning calorimetry (DSC). This system includes the Rb_3PrBr_6, Rb_2PrBr_5 and $RbPr_2Br_7$ compounds and three eutectics. Rb_3PrBr_6 undergoes a solid–solid phase transition at 704 K and melts congruently at 995 K. Rb_2PrBr_5 melts incongruently at 803 K with formation of solid Rb_3PrBr_6 and finally $RbPr_2Br_7$ melts congruently at 852 K. The electrical conductivities of $PrBr_3$–RbBr liquid mixtures measured over an extended temperature range and on the whole composition range are indicative of octahedral $PrBr_6^{3-}$ complexes formation.

Acknowledgements

Financial support by the Polish Ministry of Science and Higher Education from budget on science in 2007–2010 under the grant No. N204 4098 33 is gratefully acknowledged.

L.R., M.B. and E.I.-S. wish to thank the Ecole Polytechnique de Marseille for hospitality and support during this work.

References

[1] R. Acevedo, A. Soto-Bubert, P. Bosch, W. Strek, J. Alloys Compd. 461 (2008) 53–57.
[2] G. Oczko, L. Macalik, J. Legendziewicz, J. Hanuza, J. Alloys Compd. 380 (2004) 327–336.
[3] K.W. Kramer, P. Dorenbos, H.U. Gudel, C.W.E. van Eijk, J. Mater. Chem. 16 (2006) 2773–2780.
[4] V.B. Motalov, M.F. Butman, L.S. Kudin, K.W. Kramer, L. Rycerz, M. Gaune-Escard, J. Mol. Liq. 142 (2008) 78–82.
[5] P. Dorenbos, E.V.D. van Loef, A.P. Vink, E. van der Kolk, C.W.E. van Eijk, K.W. Kramer, H.U. Gudel, W.M. Higgins, K.S. Shah, J. Lumin. 117 (2006) 147–155.
[6] T. Markus, U. Nieman, K. Hilpert, J. Phys. Chem. Solids 66 (2005) 372–375.
[7] J. Cybinska, J. Legendziewicz, G. Boulon, A. Bensalah, G. Meyer, Opt. Mater. 28 (2006) 41–52.
[8] E.C. Guest, S.A. Mucklejohn, B. Preston, J.B. Rouffet, G. Zissis, Proceedings of International Symposium on Ionic Liquids in Honour of Marcelle Gaune-Escard, Carry le Rouet, France, June 26–28, 2003, pp. 37–45.
[9] L. Rycerz, Scientific Papers of Institute of Inorganic Chemistry and Metallurgy of Rare Elements: Series Monographs 35, Wroclaw University of Technology, Wroclaw, 2004.

[10] E. Ingier-Stocka, L. Rycerz, S. Gadzuric, M. Gaune-Escard, J. Alloys Compd. 450 (2008) 162–166.
[11] L. Rycerz, E. Ingier-Stocka, S. Gadzuric, M. Gaune-Escard, Z. Naturforsch. 62a (2007) 197–204.
[12] L. Rycerz, E. Ingier-Stocka, S. Gadzuric, M. Gaune-Escard, J. Alloys Compd. 450 (2008) 175–180.
[13] E. Ingier-Stocka, L. Rycerz, M. Berkani, M. Gaune-Escard, J. Mol. Liq. 148 (1) (2009) 40–44.
[14] J. Rejek, L. Rycerz, E. Ingier-Stocka, M. Gaune-Escard, J. Chem. Eng. Data (2010), doi:10.1021/je900891s.
[15] Y. Fouque, M. Gaune-Escard, W. Szczepaniak, A. Bogacz, J. Chim. Phys. 75 (1978) 361–366.
[16] G.I. Janz, J. Phys. Chem. Ref. Data 2 (1988) 17.
[17] G.M. Photiadis, B. Borresen, G.N. Papatheodorou, J. Chem. Soc. Faraday Trans. 94 (1998) 2605–2613.
[18] L. Rycerz, M. Gaune-Escard, unpublished results.